



# Method for visualizing under-coating corrosion utilizing pH indicators before visible damage

Can Berk Uzundal, Burak Ulgut\*

Faculty of Science, Department of Chemistry, Bilkent University, 06800 Ankara, Turkey

## ARTICLE INFO

### Keywords:

Hydrogen permeation  
Corrosion  
Corrosion detection  
Coatings  
Under-coating corrosion  
Defect visualization

## ABSTRACT

A new method for under-coating corrosion visualization is developed. The method detects corrosion through local pH gradients which are visualized by pH indicators. pH gradients are induced in a setup similar to the one popularized by Devanathan. On the uncoated back side of the metal, the sample is cathodically polarized, generating hydrogen gas through electrolysis. The hydrogen generated, diffuses through the metal sample and oxidizes on the anodically polarized painted side wherever the coating develops a defect causing a decrease in the local pH. The local pH is then used in imaging the location of defects through the use of a pH indicator, before any visible corrosion damage occurs on the coated metal sample.

## 1. Introduction

Detecting under-coating corrosion is of importance in assessment of stability and integrity of coated metal samples. When fully coated, metal samples corrode sparingly. Corrosion mainly takes place in regions where cuts, cracks or scratches are present. From these positions corrosion propagates laterally and disrupts coating integrity [1]. Under operational conditions, defects in the coating can result in the failure of the system. Evaluation of coatings and their anti-corrosive properties require facile and non-destructive methods. In the literature, a variety of methods spanning Electrochemical Impedance Spectroscopy (EIS) and Scanning Electrochemical Microscopy (SECM) are present for comparison of various coating materials [2–7]. Moreover, utilizing high frequency waves such as terahertz waves or near-field microwaves, local corrosion can be detected in the bulk scale. These high frequency detection techniques, however, depend on the dielectric differences between the paint, metal and the metal oxide which limits their applications as in the case of aluminum plates where dielectric constants are similar [8,9]. With these high frequency techniques, formation of the metal oxide cannot be visualized before a significant amount of metal oxide forms and the paint swells, thus severely limiting their detection capabilities.

Employing EIS approaches to detect under paint corrosion can deduce the effects of somewhat local changes through changes in the parameters of equivalent circuit models. Yet, the precise location of the change cannot be found on the metal plate. Truly local information on under-coating corrosion can be obtained by SECM. SECM however, requires sophisticated equipment and is not readily available for

routine analysis. Further, scanning large areas in SECM requires a long time and very large equipment. In fact, an SECM study conducted on aluminum alloys which show generation of  $H_2$  and  $H^+$  at regions of coating defects due to exposed metal sites, inspired us in developing our methodology [3,7].

In our methodology, partially inspired by the work of Devanathan, we sought to design our experiment around the  $H^+$  that is generated in the coating defects of the coated sample [10,11]. In the classical Devanathan experiment, a metal plate is fixed in between a two compartment cell (see Fig. 1) where on one compartment  $H_2$  is formed by a cathodic potential while on the other compartment the diffused  $H$  is oxidized into  $H^+$  by an anodic potential. On the latter, the current generated is monitored which yields the diffusion rate of  $H$ . The method since then, is standardized for measurement of diffusion coefficients in metal plates and measurement of metal plate thickness [12]. Recently methods that build on the classical Devanathan experiment to probe the oxygen reduction kinetics at a coating-metal interface was developed [13,14]. Although the reported approach can be used to assess overall coating integrity, local information cannot be deduced. In terms of local resolution, the potential of the Devanathan experiment was demonstrated via Scanning Kelvin Probe Microscopy, where hydrogen permeation through micro-domains of various metals could be discerned [15].

Herein we present a modification to the Devanathan experiment to tap into the local information inherently present through a very simple visualization method: Inspired by the work of Jin et al. where they utilize a pH indicator to visualize local regions of low pH as a result of higher catalytic activity towards methanol decomposition [16], we also

\* Corresponding author.

E-mail address: [ulgut@fen.bilkent.edu.tr](mailto:ulgut@fen.bilkent.edu.tr) (B. Ulgut).

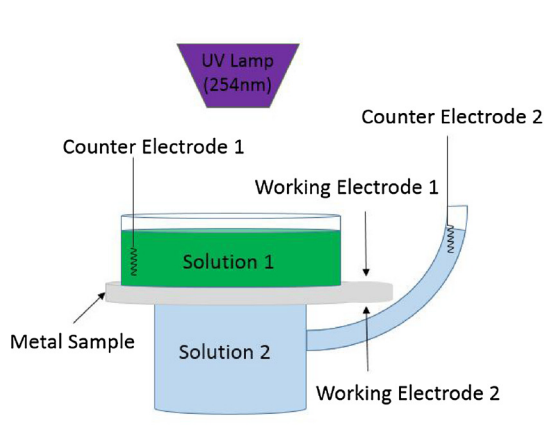


Fig. 1. Schematic representation of the setup (left). The actual setup (right).

add a pH indicator to our two compartment Devanathan setup.

## 2. Experimental

### 2.1. Method

Between the two compartments of the designed cell (see Fig. 1), a metal plate (aluminum 2024 of 0.2 mm thickness) is fixed. The bottom compartment is the generator cell where  $H_2$  is generated by a reducing potential, while the above compartment is the detection cell where the diffusing  $H$  is oxidized into  $H^+$  by an oxidizing potential. The generator cell contains saturated brine (saturated aqueous NaCl solution) while the detection cell contains brine adjusted to pH 9 or pH 6 (for phenolphthalein or quinine respectively) with NaOH. As the indicator, a couple drops of phenolphthalein or 370 mg/L quinine is added. One separate, floating potentiostat is attached to each compartment in a two electrode configuration where two graphite rods are used as both counter and reference electrodes in a two electrode configuration and the metal sample in the middle is the working electrode for both potentiostats. To the generator cell a negative constant potential is applied while to the detection cell, a small positive potential (0.5 V) is applied to generate  $H_2$  and to oxidize  $H$  into  $H^+$  respectively. Magnitude of the potential applied on the generator cell depends on the nature of the metal sample and the ability of the metal to catalyze the hydrogen formation reaction such that the metal surface is covered with hydrogen completely. As the size of the hydrogen bubble increases the current supplied drops since the electrical contact between the metal and the solution is cut off from the generator side. The complete hydrogen coverage ensures a uniform start of diffusion across the metal sample. Routinely, potentials around 10 V were applied. A constant current cannot be imposed on the metal without overloading the potentiostat attached to the generator cell since the hydrogen bubble that forms blocks the current.

Floating potentiostats are an absolute necessity in this setup since a single metal electrode acts as the working electrode of both the generator and detection cells. If two earth grounded instruments were employed, applying different potentials on the two cells would not be possible since the ground in each instrument would be fixed to the same point. Floating the potentiostats allow for the grounds of each potentiostat to be at a different level with respect to the earth ground, allowing the application of different potentials.

In our setup, a Gamry Instruments Interface 5000E was used for the generator cell and a Gamry Instruments Interface 1000E was used for the detection cell.

For experiments conducted using phenolphthalein indicator, a camera was fixed over the electrochemical cell. The fixed camera ensures that background subtraction could reliably be made.

### 2.2. Image processing

To increase the clarity of the images taken with phenolphthalein indicator, a background subtraction routine was utilized. Simply, the images are imported as arrays of RGB values (Red-Green-Blue) into a Python 2.7 environment. Each of the color channels individually are normalized using the following simple formula to account for minor changes in ambient light.

Let “C” be Red, Blue or Green Channel

$$\text{Normalized } C = \frac{C - \min(C)}{\max(C) - \min(C)} * 255$$

Then, using GIMP 2.8 image processing software, the contrast of the background subtracted images were enhanced. The contrast of an image can be thought as the difference between the brightest pixel and the darkest pixel. When the contrast of an image is increased, this difference is enhanced by making the darkest pixel darker while the brightest pixel is made brighter, where all three channels are considered in unison. The contrast enhancement was done to increase the clarity of the images such that colors can be visualized regardless of the medium this article is presented (in print or in web).

For a select case, color reduction was employed to even further enhance the contrast of the images. The GIMP algorithm for color reduction is based on the following simple algebra [17];

Let “C” be the array of values corresponding to Red, Green or Blue channels with floating point values ranging between 0 and 1

$$\text{Color reduced } C = \text{round} \left( \frac{C * \# \text{ of colors}}{\# \text{ of colors}} \right)$$

where “# of colors denote” the number of colors in the color reduced image.

Quantification shown in Fig. 7, is made easier using color reduction where color reduction lumps colors within a close region of color space to a single color. The size of this region is determined by the number of colors specified. Using color reduction, slight off-colors are assigned as pure green and can be accounted for in the quantification. Similar to contrast enhancement, color reduction also increases the clarity of the article in different media.

After normalization and color reduction (where applicable) the first image is subtracted from rest of the images by a simple array operation.

Throughout the article and the supporting information, the images are presented with their originals and their processed version.

In terms of quantification of the color reduced images, a 300-pixel by 300-pixel region was selected (shown in Fig. 7). If all the pixels in the region was purely green, the total green content of the region would be  $300 \times 300 \times 255$  where the color in any channel can be a number ranging from 0 to 255. Thus, summing the green channels of all the

pixels in the region and normalizing with respect to  $300 \times 300 \times 255$ , we can get a relative quantification on the amount of green in the region as shown in Fig. 7.

### 2.3. Materials

For metal plates of different sizes, two different cells were used throughout the experiments with the same basic schematic shown in Fig. 1. The larger cell had a detection cell outer diameter of 8 cm, the smaller cell had a detection cell outer diameter of 3.5 cm.

The experiments with the white plate and the bare metal were done using the small cell while the experiment involving the epoxy coated metal sample was conducted using the large cell due to the size differences of the samples.

Following mechanical abrasion with sandpaper (grit size P120), the metal samples were either exposed to polarization directly, or were coated with Bison 5-min epoxy (Goes, The Netherlands) prior to being exposed to polarization. The epoxy coated samples had a total thickness of 1.6 mm. The white painted sample was procured from a local supplier.

## 3. Results and discussions

### 3.1. The methodology

As mentioned in the introduction, following the SECM report that shows the evidence of elevated  $H_2$  generation in the defects of coated samples, we speculated that  $H^+$  could be generated in the reverse fashion, if  $H_2$  is present in sufficient amounts [3,7]. We utilize a Devanathan-like cell where  $H_2$  is generated in the generator cell. The generated  $H_2$  diffuses through the metal matrix and travels to the detection compartment due to the  $H_2$  concentration gradient. When the diffused  $H$  encounters the oxidizing potential of the detection cell, it is oxidized into  $H^+$ . This oxidation is expected to occur at exposed metal sites where the metal site catalyzes the reaction. Even if  $H^+$  is formed in regions without defects, the  $H^+$  is expected to diffuse laterally to the defect sites where it is exposed to the solution containing pH indicator. The  $H^+$  generated locally results in regions of low pH which is visualized by the pH indicator as can be seen in Figs. 2–4.

### 3.2. Choice of indicator

Our initial experiments used phenolphthalein as the indicator of choice simply due to its availability. Broadly, in around a minute, we saw the disappearance of the pink color upon the applied potentials thus indicating the generation of  $H^+$  as expected (Fig. 2). The loss of

color, however, is hard to identify to the naked eye except when it occurs in bulk. Emergence of a color, on the other hand, would be straightforward to identify, especially if the color occurs from a transparent solution. An indicator that covers all these bases is quinine. Under UV, it is fluorescent at acidic conditions while being non-fluorescent under basic conditions ( $pK_a = 4.5$ ).

The major problem with quinine is its fluorescence quenching in the presence of halides, in particular chloride [18]. Since corrosion studies in sea-water/salt-water is industrially relevant in assessment of coating integrity, using quinine is not suitable for these applications. Further, metals coated with 5-min epoxy, any kind of non-uniformity (bubbles, scratches etc.) and most  $TiO_2$  based white paints are fluorescent under UV (254 nm), which interferes with the observation of fluorescence from quinine. Still, as a proof-of-concept to showcase the methods ubiquity in terms choice of indicator, the detection cell was filled with 0.1 M  $Na_2SO_4$  containing 100 mg/L quinine. As prepared, the solution is not fluorescent (pH 6). Upon applied potential, however, fluorescence clearly emerges as shown in Fig. 3. Similar experiments conducted with brine only shows faint fluorescence which is hard to observe (Fig.-S1). The chloride quenching limiting the applicability of the method and coating defects being fluorescent urged us to pursue an alternative indicator for our method.

### 3.3. Background subtraction

Reflecting back on the experiments with phenolphthalein, where apparent color changes were occurring, the only hurdle was our inability to observe the loss of color from the background pink of the indicator. If we were to remove this pink background, we would effectively change the response of the indicator from a color loss to an emergence of color. Fixing a camera to a certain position and then subtracting the first image (where no potential is applied) enabled us to observe localized color changes.

Fig. 4 serves as a proof of concept where a metal sample (cleaned by mechanical abrasion grit size P120) is exposed to the procedure in the presence of phenolphthalein in brine adjusted to pH = 9 with NaOH (see S1 for time lapse animation). Due to the background subtraction, loss of pink/red is characterized by its complementary color, green. The red/pink spots in the background subtracted images signify elevated pH compared to the initial solution which is usually due to the counter reaction. As expected, for the bare metal,  $H^+$  generation occurs throughout the solution uniformly as indicated by the overall green color of the background subtracted image.

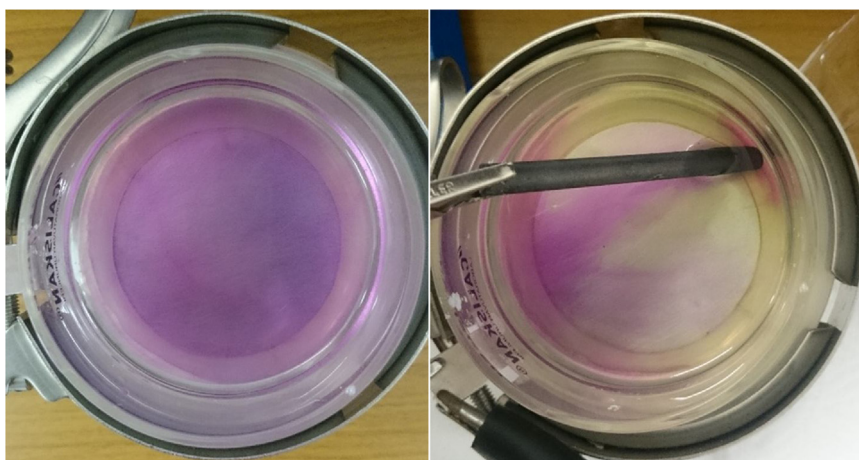
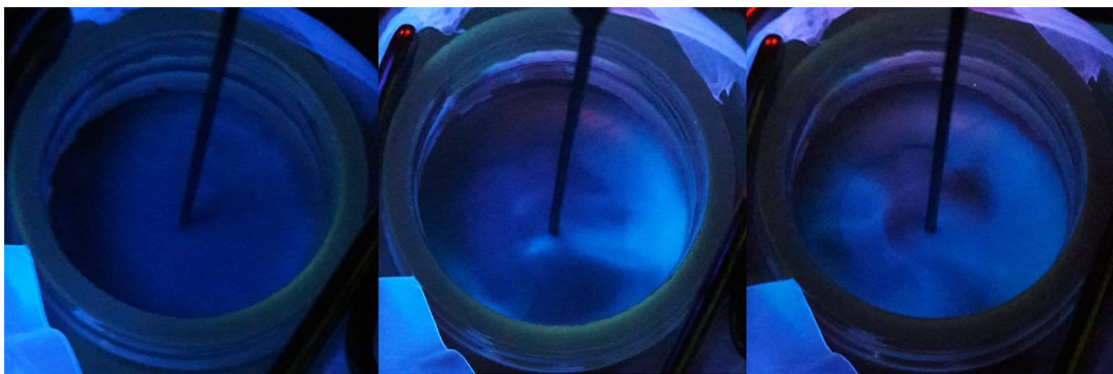
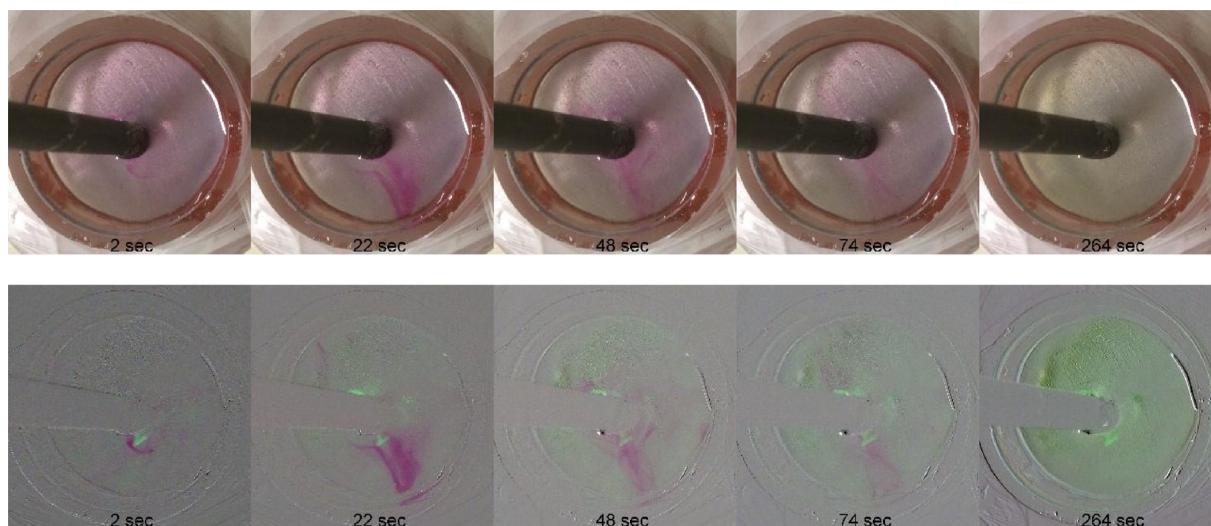


Fig. 2. The initial experiments with phenolphthalein indicator. Loss of bulk color can be seen on the right.





**Fig. 3.** Bare metal with 0.1 M  $\text{Na}_2\text{SO}_4$  containing 100 mg/L quinine, the initial picture without any fluorescence and the emergence of fluorescence with applied potential.



**Fig. 4.** Background subtracted images (bottom), unsubtracted images (top). Green color indicates regions of low pH while red indicates an increase in pH. (See S2 for time lapse animation). (For interpretation of the references to colour in this figure legend, the reader is referred to the web version of this article.)

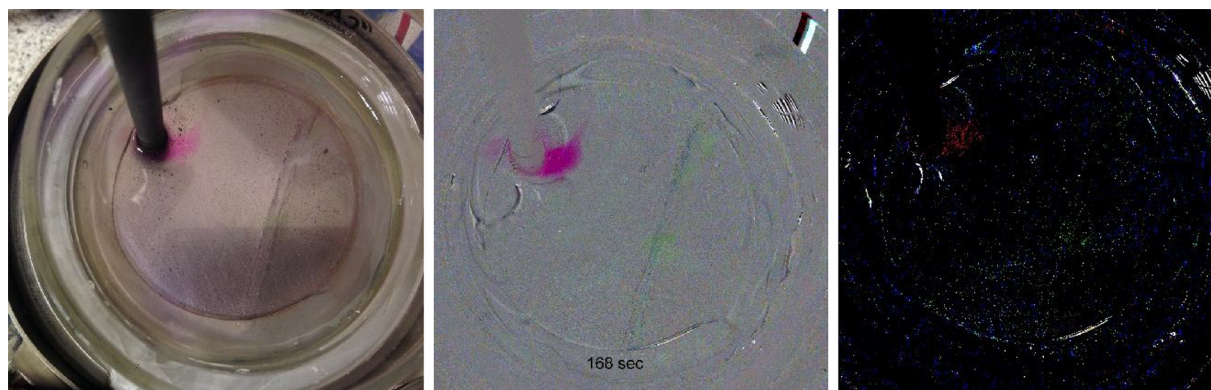


**Fig. 5.** The original image (left), background subtracted image (middle), background subtracted image with number of colors reduced to 4 (right).

### 3.4. Visualization of local pH gradients with phenolphthalein indicator

To test whether we can observe the color change locally, we used a 5-min epoxy coated metal sample with a cut. To improve the clarity of images, after background subtraction we reduced the number of colors in the image to 4. Though even in the background subtracted image faint green spots were visible, in the color reduced image the locations of lower pH are more evident (Fig. 5). Moreover, to minimize the effect of the counter reaction on visualization, we moved our counter electrode to the opposite corner. The color reduced images in Fig. 6 (see S3

for time lapse animation), shows evidence of lower pH regions along the cut on the epoxy. No visible corrosion is yet seen, however at the end of the experiment, visible corrosion occurs along the cut. Thus, with background subtraction corrosion can be observed prior to any visual confirmation beyond the local pH changes.

It is possible to quantify the green intensity locally along the cut as demonstrated by Fig. 7, where we selected a square region on the cut and plotted the amount of green in it. The intensity is normalized such that if all the pixels in the square are fully green, intensity would be 1.0. After about 450 s, significant increase in green intensity can be



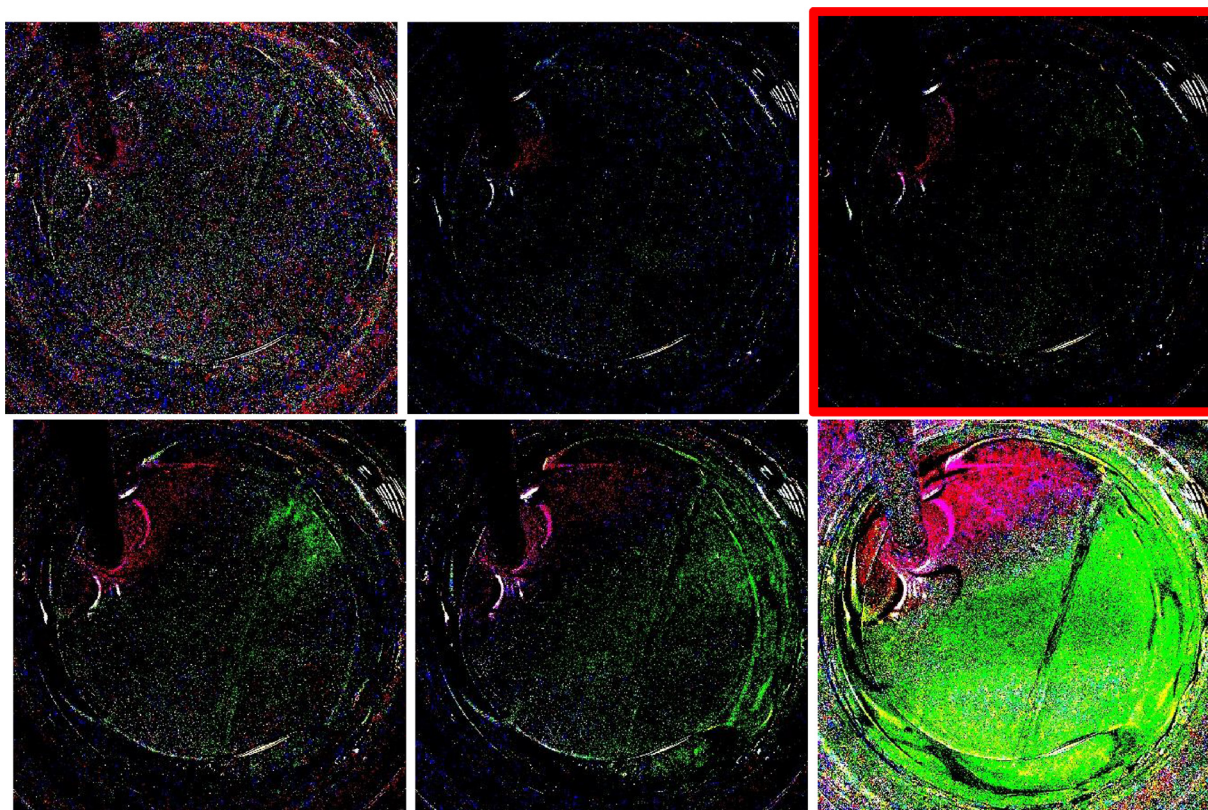


Fig. 6. Epoxy with a cut, a local pH change along the cut can be observed, especially for the image marked. (See S3 for time lapse animation).

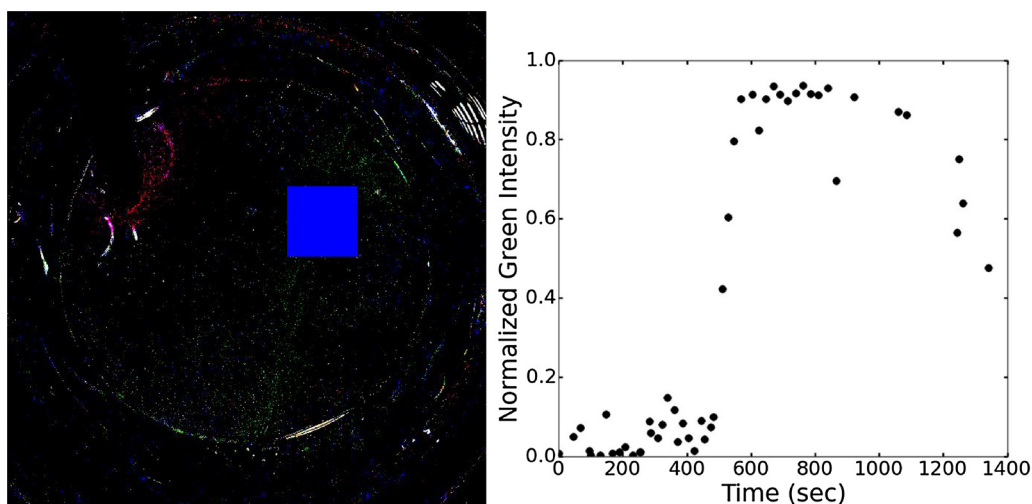


Fig. 7. The image of the monitored region, marked by the blue square (left). The normalized green intensity in the region as a function of time (right). (For interpretation of the references to colour in this figure legend, the reader is referred to the web version of this article.)

quantified.

Another challenge tackled was the observation of corrosion before any visual signs occur on painted samples. The panel used was a white painted panel that is manufactured as a test piece for household refrigerators (Fig. 8 and see S4 for time lapse animation). The paint that is used is based on  $\text{TiO}_2$  as the main pigment which is highly fluorescent. Therefore, the quinine method aside from the quenching issues was not applicable in this case. A small spot that corrodes visibly in Fig. 8, can be visualized using the local pH change prior to visible confirmation using the phenolphthalein method. This is both due to the increased intensity of the green around the location and the inherent increased clarity of the background subtracted image. To unambiguously show

the lower pH around the visibly corroding region, we again monitored two regions of color reduced images throughout time. Fig. 9 (red curve vs black curve) clearly shows that the region that corrodes at the end of the experiment gives larger green color intensities throughout time compared to a region where no visible corrosion occurs.

#### 4. Conclusions

A new method for monitoring under-paint corrosion was developed. The developed method utilizes a two compartment Devanathan cell to generate  $\text{H}^+$  at the coating defects. These local acidic regions are visualized using simple pH indicators. The basics of the method is



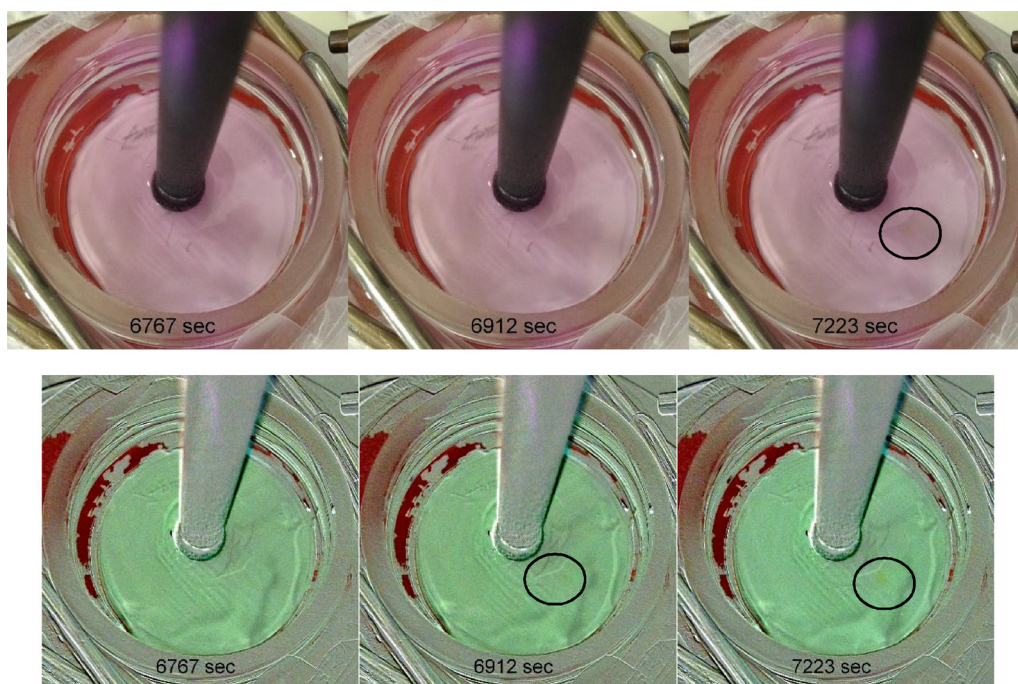


Fig. 8. White plate without background subtraction (top), with background subtraction (bottom). The corrosion can be detected earlier using background subtraction. (See S4 for time lapse animation).

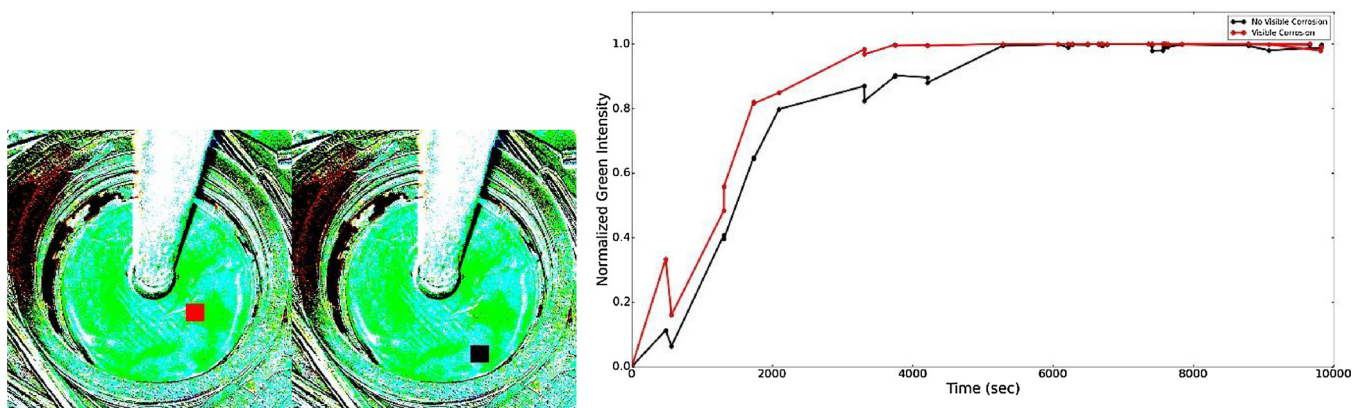


Fig. 9. Posterized images of the white plate with phenolphthalein indicator. The red square and the curve shows the visibly corroding region and its green intensity as a function of time while the black square and the curve shows a region without visible corrosion at the end of the experiment. (For interpretation of the references to colour in this figure legend, the reader is referred to the web version of this article.)

illustrated using two different indicators that are suitable for samples with varying degrees of fluorescence.

Moreover, a background subtraction routine was developed to accurately monitor local color changes especially for phenolphthalein indicator where loss of color is hard to follow. Though two examples were discussed in this paper in terms of indicators, it is possible to generalize the method for any indicator with the appropriate excitation to tailor for specific cases.

The method is shown to be successful in visualizing local corrosion behavior of coated metal samples where the currently available methods in the literature either lack the local information or require extremely long scans for local information on the bulk scale.

#### Acknowledgements

The authors gratefully acknowledge Gamry Instruments Inc. for financial support and Mr. Max Yaffe of Gamry Instruments for the original inspiration. We also thank Reviewer 2 for the remarks regarding quinine fluorescence quenching.

#### Appendix A. Supplementary data

Supplementary data associated with this article can be found, in the online version, at <https://doi.org/10.1016/j.porgcoat.2018.05.011>.

#### References

- [1] X.G. Zhang, Under-Paint corrosion, *Corros. Electrochem. Zinc*, 1st ed., Springer Science, New York, 1996, pp. 315–336.
- [2] P.L. Bonora, F. Deflorian, L. Fedrizzi, Electrochemical impedance spectroscopy as a tool for investigating underpaint corrosion, *Electrochim. Acta* 41 (1996) 1073–1082.
- [3] M.B. Jensen, A. Guerard, D.E. Tallman, G.P. Bierwagen, Studies of electron transfer at aluminum alloy surfaces by scanning electrochemical microscopy, *J. Electrochem. Soc.* 155 (2008) C324, <http://dx.doi.org/10.1149/1.2916734>.
- [4] G.P. Bierwagen, Reflections on corrosion control by organic coatings, *Prog. Org. Coat.* 28 (1996) 43–48, [http://dx.doi.org/10.1016/0300-9440\(95\)00588-9](http://dx.doi.org/10.1016/0300-9440(95)00588-9).
- [5] M. Yan, C.A. Vetter, V.J. Gelling, Corrosion inhibition performance of polypyrrole Al flake composite coatings for Al alloys, *Corros. Sci.* 70 (2013) 37–45, <http://dx.doi.org/10.1016/j.corsci.2012.12.019>.
- [6] H. Ochs, J. Vogelsang, G. Meyer, Enhanced surface roughness of organic coatings due to UV-degradation: an unknown source of EIS-artifacts, *Prog. Org. Coat.* 46

- (2003) 182–190, [http://dx.doi.org/10.1016/S0300-9440\(03\)00004-3](http://dx.doi.org/10.1016/S0300-9440(03)00004-3).
- [7] W. Shi, S.B. Lyon, Investigation using localised SVET into protection at defects in epoxy coated mild steel under intermittent cathodic protection simulating intertidal and splash zones, *Prog. Org. Coat.* 102 (2017) 66–70, <http://dx.doi.org/10.1016/j.porgcoat.2016.04.035>.
- [8] R.F. Anastasi, E.I. Madaras, Terahertz NDE for under paint corrosion detection and evaluation, *AIP Conf. Proc.* 820I (2006) 515–522, <http://dx.doi.org/10.1063/1.2184571>.
- [9] D. Hughes, Microwave nondestructive detection of corrosion under thin paint and primer in aluminum panels, *AIP Conf. Proc.* 557 (2001) 460–466, <http://dx.doi.org/10.1063/1.1373793>.
- [10] M.A.V. Devanathan, Z. Stachurski, The mechanism of hydrogen evolution on iron in acid solutions by determination of permeation rates, *J. Electrochem. Soc.* 111 (1964) 619–623, <http://dx.doi.org/10.1149/1.2426195>.
- [11] M.A.V. Devanathan, Z. Stachurski, The adsorption and diffusion of electrolytic hydrogen in palladium, *Proc. R. Soc. A Math. Phys. Eng. Sci.* 270 (1962) 90–102, <http://dx.doi.org/10.1098/rspa.1962.0205>.
- [12] American Society for Testing Materials, Standard Practice for Evaluation of Hydrogen Uptake, Permeation, and Transport in Metals by an Electrochemical Technique vol. G148-97. i, (2011), pp. 1–10, <http://dx.doi.org/10.1520/G0148-97R11>.
- [13] D. Vijayshankar, A. Altin, C. Merola, A. Bashir, E. Heinen, M. Rohwerder, Probing the buried metal-organic coating interfacial reaction kinetic mechanisms by a hydrogen permeation based potentiometric approach, *J. Electrochem. Soc.* 163 (2016) C778–C783, <http://dx.doi.org/10.1149/2.0971613jes>.
- [14] D. Vijayshankar, T.H. Tran, A. Bashir, S. Evers, M. Rohwerder, Hydrogen permeation as a tool for quantitative characterization of oxygen reduction kinetics at buried metal-coating interfaces, *Electrochim. Acta* 189 (2016) 111–117, <http://dx.doi.org/10.1016/j.electacta.2015.12.030>.
- [15] S. Evers, M. Rohwerder, The hydrogen electrode in the dry: a Kelvin probe approach to measuring hydrogen in metals, *Electrochem. Commun.* 24 (2012) 85–88, <http://dx.doi.org/10.1016/j.elecom.2012.08.019>.
- [16] J. Jin, M. Prochaska, D. Rochefort, D.K. Kim, L. Zhuang, F.J. DiSalvo, R.B. van Dover, H.D. Abruña, A high-throughput search for direct methanol fuel cell anode electrocatalysts of type Pt<sub>x</sub>Bi<sub>y</sub>Pb<sub>z</sub>, *Appl. Surf. Sci.* 254 (2007) 653–661, <http://dx.doi.org/10.1016/j.apsusc.2007.06.077>.
- [17] GIMP Source Code, (2017) <https://www.gimp.org/source/#gimp-source-code/>. (Accessed 7 November 2017).
- [18] B. Verity, S.W. Bigger, The dependence of quinine fluorescence quenching on ionic strength, *Int. J. Chem. Kinet.* 28 (1996) 919–923, [http://dx.doi.org/10.1002/\(SICI\)1097-4601\(1996\)28:12<919::AID-KIN9>3.0.CO;2-Q](http://dx.doi.org/10.1002/(SICI)1097-4601(1996)28:12<919::AID-KIN9>3.0.CO;2-Q).